Published in final edited form as:
Biomaterials. 2012 February ; 33(5): 1500–1508. doi:10.1016/j.biomaterials.2011.10.068.

An activatable multimodal/multifunctional nanoprobe for direct imaging of intracellular drug delivery

Rajendra N. Mitra[a], **Mona Doshi**[a], **Xiaolei Zhang**[b,c], **Jessica C. Tyus**[d], **Niclas Bengtsson**[e], **Steven Fletcher**[f], **Brent D. G. Page**[f], **James Turkson**[c], **Andre J. Gesquiere**[a,d,g], **Patrick T. Gunning**[f], **Glenn A. Walter**[h], and **Swadeshmukul Santra**[a,b,d,*]

[a]NanoScience Technology Center, University of Central Florida 12424 Research Parkway, Suite 400, Orlando, FL 32826, USA

[b]Biomolecular Science Center, University of Central Florida 12424 Research Parkway, Suite 400, Orlando, FL 32826, USA

[c]Burnett School of Biomedical Sciences, University of Central Florida College of Medicine, 6900 Lake Nona Boulevard, Orlando, FL 32827, USA

[d]Department of Chemistry, βCREOL, The College of Optics and Photonics, and the, 12424 Research Parkway, Suite 400, Orlando, FL 32826, USA

[e]Molecular Genetics and Microbiology, University of Florida, PO Box 100201, Gainesville, FL 32610, USA

[f]Department of Chemistry, University of Toronto at Mississauga, Mississauga, ON, L5L 1C6, Canada

[g]CREOL, The College of Optics & Photonics, University of Central Florida, P.O. Box 162700, Orlando, FL 32816, USA

[h]Physiology and Functional Genomics, University of Florida, PO Box 100274, Gainesville, FL 32610, USA

Abstract

Multifunctional nanoparticles integrated with imaging modalities (such as magnetic resonance and optical) and therapeutic drugs are promising candidates for future cancer diagnostics and therapy. While targeted drug delivery and imaging of tumor cells have been the major focus in engineering nanoparticle probes, no extensive efforts have been made towards developing sensing probes that can confirm and monitor intra-cellular drug release events. Here, we present quantum dot (Qdot)-iron oxide (IO) based multimodal/multifunctional nanocomposite probe that is optically and magnetically imageable, targetable and capable of reporting on intra-cellular drug release events. Specifically, the probe consists of a superparamagnetic iron oxide nanoparticle core (IONP) decorated with satellite CdS:Mn/ZnS Qdots where the Qdots themselves are further functionalized with STAT3 inhibitor (an anti-cancer agent), vitamin folate (as targeting motif) and m-polyethylene glycol (m-PEG, a hydrophilic dispersing agent). The Qdot luminescence is quenched in this nanocomposite probe (“OFF” state) due to combined electron/energy transfer mediated

*To whom all correspondence should be made. ssantra@mail.ucf.edu.

Appendix. Supplementary materials Supplementary materials associated with this article can be found, in the online version.

quenching processes involving IONP, folate and STAT3 agents. Upon intracellular uptake, the probe is exposed to the cytosolic glutathione (GSH) containing environment resulting in restoration of the Qdot luminescence ("ON" state), which reports on uptake and drug release. Probe functionality was validated using fluorescence and MR measurements as well as in vitro studies using cancer cells that overexpress folate receptors.

Keywords

magnetic nanoparticles; quantum dots; targeted drug delivery; bioimaging; biosensing

1. Introduction

Cancer nanotechnology focuses mainly on two key aspects, disease diagnostics and therapy[1, 2]. Studies have shown that engineered nanoparticles, integrated with multimodality/multifunctionality, are capable of imaging cancer cells with high sensitivity and successfully deliver pre-loaded therapeutic drugs to tumors in a targeted manner[3–7]. For example, multimodal nanoparticles with optical and magnetic imaging modalities[8–13] are expected to facilitate pre-operative cancer diagnosis by MRI and optical based imaging[14–18], to provide intra-operative surgical guidance (by optically demarcating tumor tissue from healthy tissue) and to track tumor metastasis[2, 7, 8]. In spite of these developments, no major breakthrough in nanoparticle engineering has been made for direct imaging of intracellular drug delivery events. Current nanoparticle technology allows for imaging of particles carrying therapeutic drugs[3, 6, 7, 14, 19, 20]. However, no activatable drug delivery system has been reported to date that has demonstrated the ability to directly confirm intracellular drug release upon reaction with a cytosolic biomolecule.

Up until now, challenges in designing and constructing a nanoparticle integrating imaging, monitoring, and therapeutic functionalities in a single unit have restricted the fabrication of such a nanoparticle system. To address this challenge, development of an activatable multifunctional/multimodal composite nanoprobe (MMCNP) that has the capability of optical tracking of the intracellular release of therapeutic drugs is highly desirable. It is also desirable to integrate such MMCNP with MR imaging modality and cancer targeting functionality.

Here, we present quantum dot (Qdot)-iron oxide (IO) based MMCNP that is optically and magnetically imageable, targetable and capable of reporting on intracellular drug release events. Activatable optical based functionality integrated with MRI modality forms a basis of the MMCNP design that will allow monitoring of the intracellular drug release event. Recent literature reports[21–27], including our previous studies[25, 26], demonstrate that luminescence of quantum dots (Qdots) can be drastically quenched by conjugating them with electron-rich ligands. This quenching is attributed to a combined electron/energy transfer process between the ligands and Qdots. Qdot luminescence will be restored once surface-bound ligands are detached from Qdots or the quenching processes are stopped. A number of Qdot sensing probes that are designed based on Fluorescence Resonance Energy Transfer (FRET) mechanism have been reported[21, 23, 24, 28] demonstrating feasibility of using Qdot as one of the FRET pair. Bagalkot et al. reported a bi-FRET based construct of Qdot-aptamer-drug (doxorubicin) where the drug was intercalated with the aptamer and fluorescence of both Qdot and doxorubicin were quenched[28]. The limitation of this bi-FRET construct design is that the drug is not directly attached to the fluorescence reporter and therefore establishment of exact drug release mechanism is challenging. Moreover, this design would not confirm the release of drugs in cytosolic environment which is desirable.

The present MMCNP probe, however, takes advantage of Qdot based optical "OFF/ON" reporting mechanism[25] where the drug was directly attached to the Qdot. Specifically, the probe consists of a superparamagnetic iron oxide nanoparticle core (IONP) decorated with satellite CdS:Mn/ZnS Qdots where the Qdots themselves are further functionalized with STAT3 inhibitor (an anti-cancer agent), vitamin folate (as targeting motif) and m-polyethylene glycol (m-PEG, a hydrophilic dispersing agent). The Qdot luminescence is quenched in this nanocomposite probe ("OFF" state) due to combined electron/energy transfer mediated quenching processes involving IONP, folate and STAT3 agents. Upon intracellular uptake, the probe is exposed to the cytosolic biomolecule, glutathione (GSH) containing environment resulting in restoration of the Qdot luminescence ("ON" state), which reports on uptake and drug release. Probe functionality was validated using fluorescence and MR measurements as well as in vitro studies using cancer cells that overexpress folate receptors.

The multimodal/multifunctional nanocomposite probe and proof-of-concept studies thereof presented in this paper are expected to strengthen future nanomedicine research by improving our ability to design sensitive `targeted cell-shuttle" type nanoprobes for monitoring drug delivery and therapy. This strategy provides a new nanotechnology enabled tool that has strong potential to facilitate drug discovery.

2. Materials and methods

2.1. The MMCNP design and synthesis

The MMCNP consists of a super-paramagnetic iron oxide nanoparticle core (IONP; ~ 5 – 20 nm size) and satellite CdS:Mn/ZnS quantum dot (Qdots; ~ 3.5 nm size) shell (Scheme 1). Each Qdot was attached to the core IONP by a hetero-bifunctional cross-linker molecule, dihydrolipoic acid (DHLA). The DHLA connected the IONP through its carboxyl end and the Qdot via its bidantate thiol bonds. To minimize the possibility of cross-linking, the IONP-Qdot conjugation strategy involved controlled addition of DHLA modified IONP to unmodify Qdots as described in the experimental section. The carboxyl and the thiol functional groups are compatible with the IONP and Qdot particle surfaces, respectively[23, 29–31].

Upon attachment of a Qdot to a IONP nanocrystal, a large surface area still remained available on the satellite Qdots for further surface modification and conjugation. Next, an N-acetyl-L-cysteine (NAC) modified STAT3 inhibitor (NAC-STAT3; a therapeutic model drug), a NAC modified folate (NAC-FA; a cancer targeting agent) and a NAC modified ethylenediamine (NAC-EDA, an amine modified ligand) were separately synthesized. NAC mediated surface modification of Qdots has several advantages: (i) it passivates the Qdot surface via formation of stable disulfide bonds, resulting in increased quantum efficiency, (ii) it improves aqueous dispersibility of Qdots, and (iii) it provides surface carboxyl groups for functionalization with other desired ligands. Furthermore, this approach reflects the uniqueness of the reported MMCNP design, where the separate synthesis of each of these ligands allows for control of the ratio of these ligands when attaching to Qdots or substitution of one of these ligands, resulting in a fully modular design of the MMCNP (nanoparticle LEGO®). After IONPQdot conjugation, further surface conjugation reactions were performed by treating IONP-Qdot with a mixture of NAC-STAT3, NAC-FA and NAC-EDA. The surface modification procedures are mentioned in detail in the experimental section. The surface amine groups (provided by NAC-EDA) were reacted with the N-hydroxysuccinimide (NHS) ester derivative of methyl-poly-ethylene glycol (mPEG-NHS ester; a highly-hydrophilic dispersing agent) to improve overall dispersibility of the MMCNPs.

STAT3 drug and FA were intentionally selected as electron-rich ligands that can quench Qdot fluorescence. This selection process involved simple mixing of each of these ligands with Qdots followed by observation of the extent of luminescence quenching (data not shown). Each of these ligands thus served a dual purpose. The treatment of IONP-Qdots with NAC-STAT3 and NAC-FA drastically reduced the rest of the fluorescence of the Qdots. It was noted that NAC itself did not quench Qdot luminescence, thus justifying the combined role of STAT3 drug and FA as quenchers. As a result, the MMCNP was essentially in a fluorescently quenched ("OFF") state. The luminescence of MMCNPs was restored ("ON" state) upon treatment with an appropriate agent, that effectively cleaves disulfide bonds between the ligand and the IONP-Qdots, such as GSH.

2.2. Materials

All the chemicals were used as received. Ferric (III) chloride hexahydrate, Ferrous (II) chloride tetrahydrate, ethylenediamine were purchased from Fluka. Lipoic acid, Sodium borohydride were purchased from Sigma-Aldrich. Methyl-PEG-12-NHS and Folic acid were purchased from Fisher. All the other chemicals and solvents were purchased from Fisher. The Nanopure water was used for our study. Fluorescence spectra were recorded in NanoLog Spec Fluorimeter, Perkin Elmer. The FTIR spectra were recorded in Perkin Elmer Spectrum 100. UV-Vis spectra were recorded in Cary Win UV spectrometer. The low and high resolution electron microscopic images were taken in TEM JEOL 1011 and FEI Tecnai F30 TEM instruments respectively.

2.3. Method

2.3.1. STAT3 inhibitor (SF-1-046, drug)—The non-phosphorylated salicylic acid-based small-molecule, SF-1-046, belongs to the S3I-201.1066 class of STAT3 inhibitors[32, 33]. Compounds in this class, including SF-1-046, are structural analogs of the previously reported lead STAT3 dimerization disruptor, S3I-201[34]. Consistent with the published reports regarding the activities of the lead and the other members of the second generation class of compounds[32–34], GOLD computational modeling[35] indicated SF-1-046 interacts with the STAT3 SH2 domain (data not shown), disrupting STAT3 SH2 domain:pTyr interactions, and thereby inhibit Stat3 activation. SF-1-046 was prepared via previously published synthetic protocols[32, 33].

2.3.2. Synthesis and Surface Modification of IONPs by Dihydrolipoic acid—The Super Paramagnetic Iron Oxide nanoparticles (IONPs) were prepared following the previous established protocol[36]. In brief, we have taken 1.0 M (1.13g) of ferric chloride hexahydrate ($FeCl_3 \cdot 6H_2O$) and 0.5 M (0.415g) ferrous (II) chloride tetrahydrate ($FeCl_2 \cdot 4H_2O$), 0.177 mL of 37% HCl were taken in 4 mL of DI water and stirred vigorously in a vortex in 15 mL centrifuge tube. 1.66 mL of 28–30% NH_4OH solution was dissolved in 31 mL of DI water in a conical flask and stirred vigorously for 5 min. Then the ferric chloride/ferrous chloride/HCl solution was suddenly added to the stirring ammonia solution and the mixture was stirred again for 30 min with 800 rpm at room temperature in a nitrogen atmosphere to prevent critical oxidation. The black precipitate formed instantly. After complete stirring the iron oxide nanoparticles were separated by sedimentation at the bottom of the flask using external neodymium magnetic field. 15 mL of the supernatant was decanted and then again the stirring was continued at 800 rpm. 80 mg of lipoic acid (LA) was added in 20 mL chloroform and was vortexed for 20 min. This lipoic acid solution was then added to the iron oxide nanoparticle dispersion shortly. The lipoic acid was used to coat the iron oxide nanoparticles (Supplementary Materials, Fig. S6). After 4h complete stirring, 20 mL of methanol was added to reduce the viscosity of the aqueous phase and allowed the chloroform based ferrofluid to settle at the bottom of the container. The clear aqueous phase was first decanted and then the chloroform part was diluted again by 10 mL of chloroform.

The chloroform residue was then taken in a separating funnel and washed with water to neutrality. The chloroform part then taken in a 50 mL conical and dried under vaccum to get the black solid powder. Thus we obtained the lipoic acid coated iron oxide nanoparticles (LA-IO).

We were then chemically reduced the disulfide bond of LA-IO to dithiol groups. In doing that we first took 0.2g of solid black lipoic acid coated iron oxide nanoparticles in 50 mL of water/ethanol mixture (1:1) and then dispersion was ultra sonicated for 10 min followed by vigorous stirring for another 20 min in ice bath. 0.2g of ice cold solution of freshly prepared sodium borohydride was slowly added to it under vigorous stirring condition. After complete addition of the solution the stirring was continued for another 2h. The black materials are then separated by sedimentation using strong neodymium magnet and washed with DI water to neutrality. The material was then taken in choloroform and dried under vacuum to get the solid black dihydrolipoic acid coated iron oxide nanoparticles (DHLA-IO). They were used for the next step of reaction as synthesized.

2.3.3. Synthesis of CdS:Mn/ZnS Quantum dots (Qdots)—We have used purely dopant based core-shell CdS:Mn/ZnS nanocrystals for our study. The CdS:Mn/ZnS Qdots were synthesized by a water-in-oil (W/O) microemulsion method following a published protocol[37] In brief, we have taken dioctyl sulfosuccinate sodium salt (AOT)/ heptane/ water microemulsion system. In brief, cadmium acetate dihydrate ($Cd(CH_3COO)_2.2H_2O$), manganese acetate tetrahydrate ($Mn(CH_3COO)_2.4H_2O$), sodium sulfide (Na_2S), and zinc acetate dihydrate, metal basis ($Zn(CH_3COO)_2.2H_2O$) were used for the preparation of (Cd^{2+} Mn^{2+}), S^{2-}, and Zn^{2+} ions containing standard aqueous solutions. The aqueous solution was stirred for 15 min and then added to the AOT/heptane solutions to form the water-in-oil (W/O) microemulsions. The Mn-doped CdS core nanocrystals were formed by mixing (Cd^{2+} and Mn^{2+}) and S^{2-} containing (W/O) microemulsions rapidly for 10–15 min. The W_0 (water-to-surfactant ratio) value of W/O microemulsions were maintained at 10. For the growth of outer shell layer on the Mn doped CdS core Qdots, the Zn^{2+} ion containing (W/O) microemulsion was added at very slow rate (1.5 mL/min) to the (W/O) microemulsions containing CdS:Mn. The nucleation and growth of a separate ZnS phase were suppressed by the very slow addition of the Zn^{2+} containing W/O microemulsion. The [Zn^{2+}] to [Cd^{2+}] molar ratio (X_0) was 8 for our study.

2.3.4. Synthesis of NAC Derivatives of Folic Acid (FA), Drug (STAT3 inhibitor) and Ethylenediamine (EDA)—The Folic acid, drug (STAT3 inhibitor) and ethylenediamine (EDA) were separately conjugated to NAC following standard bioconjugation techniques as described below.

2.3.4.1. STAT3-NAC Conjugation: A 2 mL anhydrous DMSO solution containing 3×10^{-5} mol of N-acetyl cysteine, 5.7×10^{-4} mol of EDC and 1.5×10^{-4} mol of NHS was stirred for 30 min at room temperature. After this incubation, 1.5×10^{-5} mol of solid STAT3 inhibitor compound (contains secondary non-functional amine group) was added and whole solution mixture was stirred for 2h at room temperature. The reaction mixture was passed through 0.2μm whatman membrane and the solution was then dried under vacuum. The product was dispersed in 1 ml nanopure water.

2.3.4.2. EDA-NAC Conjugatation: Following the same procedure as above, a 2 mL anhydrous DMSO reaction mixture containing 1.2×10^{-4} mol of N-acetyl cysteine, 1.2×10^{-3} mol of EDC and 0.3×10^{-3} mol of NHS was stirred for 30 min at room temperature. After this incubation, 1.2×10^{-3} mol of ethylenediamine was added and the whole reaction mixture was then stirred for another 2h at room temperature. Then N_2 gas was passed

through it followed by filtration through a 0.2μm Whatman membrane. This solution was then dried under vaccum and the dried product was then dispersed in 1 ml nanopure water.

2.3.4.3. FA-NAC Conjugation: Following the same procedure as above, 2 mL PBS solution containing 2.8×10^{-5} mol of folic acid, and 5×10^{-5} mol of EDC was stirred for 30 min at room temperature. To this solution, 0.5 ml of the NAC-EDA complex was added. The resulting reaction mixture was then stirred for overnight in dark at room temperature. The reaction mixture was then passed through a 0.2 μm cut-off Millipore® membrane filter. This solution was then dried under vaccum and finally dispersed in nanopure water.

Synthesis of Qdots attached iron oxide nanoparticles (IONPs-Qdots). In this synthesis process we first extracted the CdS:Mn/ZnS core-shell quantum dots (Qdots) from the microemulsion solution by repeated centrifugation followed by washing several times with methanol and ethanol. The extracted Qdots were dispersible in DI water and used as extracted from microemulsion solution. To the 1mL Qdots dispersion (20mg/mL) in water, the DHLA coated IONPs dispersion (2mg/mL) in 4 mL ethanol was added dropwise. After complete addition, the whole reaction mixture was stirred for overnight. Thereafter the nanoparticles were separated by strong external neodymium magnet and washed several times with ethanol and DI water to remove the unused Qdots. In this way, the Qdots were attached on the surface of IONPs through DHLA linker. The attachment of Qdots on IONP surface, however, partially reduced the brightness of the Qdot luminescence. The IONP-Qdot composites were bright enough to be easily visualized under illumination by a hand-held 366 nm multiband UV light source. Furthermore, the IONP-Qdot composites responded well to external magnetic fields.

2.3.5. Surface Functionalization of IONPs-Qdots—The 2mg/mL IONPs-Qdots nanoparticles were taken in DMSO/ethanol (4:1) mixture and stirred as well as sonicated to disperse well. This dispersion was showing fluorescence under hand-held 366 nm multiband UV light source. This well dispersion was then added to a mixture of 0.7 mL of drug-NAC, 0.2 mL of EDA-NAC and 0.4 mL of FA-NAC conjugates slowly under contant vortexing and UV exposure. It was observed that the previous fluorescence intensity of the IONP-Qdot conjugates quenched. The reaction was stirred for overnight and then the whole conjugated nanocomposites were separated by strong external neodymium magnet and washed several times with DMSO and nanopure water. Finally the reaction mixture was dispersed in 1ml of 0.1(M) $NaHCO_3$ solution and stirred for few minutes in dark. After this stirring, 5.5 mg of methyl-PEG-NHS ester was added to it and the whole solution was stirred for overnight. These MMCNPs were then separated by external neodymium magnet and washed several times with DPBS and finally was taken in DPBS for further use.

2.3.6. Preparation of MRI samples—Human breast cancer (MDA-MB-231), pancreatic cancer (Panc-1), and mouse thymus stromal epithelial (TE-71) cells have all been previously reported[32, 33]. Cells were grown in Dulbecco's modified Eagles's medium (DMEM) containing 10% heat-inactivated fetal bovine serum. Cells were treated with nanoparticles at concentration of 0.1mg/ml for 24 hours. The medium was extracted by vacuum, and cells were washed by 1x PBS buffer for 6 times to remove the unbound nanoparticles. Cells were detached by Trypsin with 0.25% EDTA, centrifuged down at 1500 rpm for 3 minutes and then discarded supernatant. Cells were then resuspended in sterile water and mixed with equal volume 3x PBS and 3% agarose, and carefully poured into 10mm NMR tubes. Positive control was prepared by mixing 0.3mg/mL nanoparticles solution with equal volume of 3x PBS and 3% agarose.

2.3.7. Magnetic Resonance Imaging—Magnetic resonance imaging of a layered cell phantom was performed at 14T magnetic field strength using Paravision 3.0.2 software and

a 10 mm microimaging coil (Bruker). A three-dimensional gradient echo scan sequence (FLASH) was acquired with following settings; repetition time (TR) = 200 ms, echo time (TE) = 2.7ms, 128×128×128 matrix size and field of view (FOV) = 10×10×20 mm^3. Hypointense signal from clusters of iron oxide containing cells, was inverted and assigned a red pseudocolor for image presentation on subsequent 3D renderings performed using OsiriX viewing software (http://www.osirix-viewer.com).

2.3.8. CyQUANT™ Cell Proliferation Assay—The human breast cancer (MDA-MB-231) cells, or the mouse thymus epithelial stromal (TE-71) cells and pancreatic cancer (Panc-1) cells were grown in Dulbecco's modified Eagles's medium (DMEM) containing 10% heat-inactivated fetal bovine serum. 5000 Cells per well were cultured in 96-well plate. The cells treated with nanoparticles, compounds (drug), and nanoparticles were conjugated to compound for 24 hours, and then performed Cyquant cell proliferation assay (Invitrogen Corp/Life Technologies Corp, Carlsbad, CA). The medium was removed by vacuum, and add 50 μL 1×dye binding solution to each microplate well and then incubated at 37°C for 30 minutes. The fluorescence intensity of each sample was measured using a fluorescence microplate reader (POLARstar Omega, BMG Labtech, Durham, NC, USA) with excitation at about 485nm and emission detection at about 530nm.

2.3.9. Confocal Fluorescence Microscopy—The cells were fixed on the glass slide after 24 hrs of incubation with the nanoparticles. Confocal fluorescence miscroscopy on the cells was done with the home-built sample-scanning confocal microscope. The excitation source was 375nm pulse diode laser (PicoQuant GmbH, LDH-P-C-375). The power used was 3nW. The laser was focused on a spot size of ~300 nm with a Zeiss 100× Fluar objective lens (NA 1.3, WD 0.17mm). The sample was raster scanned using a piezoelectric stage (Mad City Labs, Nano- LP100) to get the fluorescence images of the cells with the quantum dots. The fluorescence was detected using the avalanche photodiode (PerkinElmer SPCM-AQR-14). The spectra were collected using a spectrograph with a grating (150 g/mm, blaze: 500 nm) centered at 600 nm (PI Acton SP-2156) which was coupled to a thermoelectrically cooled Electron Multiplying Charge Coupled Device (EM –CCD Andor iXon EM+ DU-897 BI). Spectra were collected from different spots on the cells.Each spectrum was collected with 10 sec exposure time and with three consecutive exposures. These were then averaged in the home written Matlab program (Mathwork Inc. Natick, Massachusetts). After taking such 100 averaged spectra those were compiled and an ensemble spectrum was built in Matlab program. The corresponding bright field images were taken by using the same spectrograph with grating (1200 g/mm, blaze: mirror) centered at 4 nm and coupled with EM-CCD. The exposure time for bright field image was 0.05 sec.

2.3.10. UV-Vis and Fluorescence Measurements—The UV-Vis absorption spectra were collected by using 1 cm path length quartz cuvette with Agilent 8453 spectrometer. The fluorescence emission spectra were taken by using the 1 cm path length quartz cuvettes with Nanolog™ HoribaJobin Yvon fluorimeter. The excitation and emission slits were 5 nm. The excitation wavelength was 375 nm for quantum dots and 300 nm for the drug. In 2 mL PBS, 100 μL quantum dots in PBS were added and the absorption and emission was taken. Then 50 μL of 0.3 M solution of GSH was added and absorption and emission spectra were collected immediately after addition of GSH and after every 5 min upto 60 min. This gave a plot of λ_{max} emission Vs time in min. After 35 min the fluorescence was almost constant showing that the drug is completely released after 35 min.

3.Results and Discussion

The morphological, optical, and magnetic properties of MMNCPs were extensively characterized. TEM studies confirmed the formation of 20–40 nm size nanocomposites as

shown in Fig. 1. The IONP core and satellite Qdots surrounding the core are clearly visible with low resolution TEM (Fig. 1) whereas magnified TEM images clearly show Qdots around the IONP (Fig. 1 inset). The IONP can be discerned in the image by its light grey contrast while the Qdots appeared with dark contrast on the IONP surface. Individual satellite Qdots on the IONP surface can be clearly identified by their single crystalline structure while the IONP in the HRTEM image is obscured by the satellite Qdots (Supplementary Materials, Fig. S1). Inductively coupled plasma analysis of the sample confirmed the presence of Zn (41 wt%), Fe (6.2 wt%) and Cd (10 wt%) with a relative ratio of 6.6 : 1.0 : 1.6 (W/W). Zeta potential (ξ) measurements correlated with particle surface charge. The ξ w −20 mV, −4.0 mV, −17 mV and −21 mV, respectively. As expected, DHLA modification of IONP drastically reduced its surface charge due to reduction of the negative surface charge of IONP. Further surface modification with the STAT3 drug and folic acid resulted in an increase in the overall negative surface charge on the particle. This is due to the presence of carboxyl groups on the folic acid residues on the particle surface. Pegylation with mPEG, however, showed minimal effect on the particle surface charge due to its neutral nature. It was observed that pegylated particles exhibited good phosphate buffer dispersibility. A comparative analysis of FT-IR spectra of IONP, DHLA, lipoic acid, and IONP-DHLA confirmed successful surface modification of IONP with DHLA (Supplementary Materials, Fig. S2). The broad band at 3200–3600 cm^{-1} indicates the surface hydroxyl group of the super paramagnetic IONPs (Fig. S2d). The bands at 3046 (O-H), 2934(–CH_2–), 1697 (C=O), 1252 (O-H), and 935 (OH) cm^{-1} were observed for dihydrolipoic acid and lipoic acid (Fig. S2a and b respectively). The presence of these characteristic bands into the spectra of dihydrolipoic acid coated IONPs (Fig. S2c) confirmed the dihydrolipoic acid coating on the surface of IONPs. Fluorescence spectroscopy in solution was used to investigate the Qdot luminscence properties at different stages of MMCNP development as well as for tracking the drug release event. GSH, a tripeptide biomolecule found in all animal cells at relatively high cytosolic concentration (1–10 mM[38, 39], reduced form), effectively reduces disulfide bonds and in this process glutathione is converted to glutathione disulfide (GSSG), its oxidized form.[40] The design of the MMCNPs is such that once it is exposed to the intracellular GSH environment, it will disintegrate into its different constituents that make up the composite nanoparticle. This forms the basis of the intracellular tracking of the STAT3 drug release as schematically shown in Scheme 1. Distinct changes in absorption spectra were observed for IONP-Qdot and IONP-Qdot-STAT3 conjugates in comparison to Qdots (Fig. S3a). The Qdot absorption spectrum broadens significantly and slightly shifts towards longer wavelength when conjugated to IONPs. However, upon further conjugation with NAC-STAT3 drug, NAC-FA and NAC-EDA, a decrease in spectral width along with slight blue shift was observed with respect to the IONP-Qdots conjugates. Such changes in absorption spectral characteristics support successful surface conjugation of Qdots with IONP, STAT3 drug and FA. The emission of MMCNP was slightly blue shifted compared to either Qdots or IONP-Qdot conjugates (Fig. S3b).

Fluorescence data acquired by adding GSH to MMCNPs in solution showed that Qdot fluorescence could be restored completely in less than one hour (Fig. 2) after which no further increase in Qdot fluorescence intensity was observed. The inset shows a plot of Qdot fluorescence intensity measured at the peak emission wavelength (582 nm) as a function of time. This plot illustrated that the fluorescence intensity plateaus at 60 minutes. Furthermore, a systematic study on the effect of GSH concentration on the time scale of fluorescence restoration showed that there was no significant effect of varying GSH concentrations in the range of 2.8 mM to 7 mM (Fig. S4). Even at the lowest GSH concentration, the Qdot fluorescence recovered in approximately 1 hour. Furthermore, the timescale of fluorescence recovery appeared to be independent of GSH concentration higher than 1.4 mM. Since the intracellular concentration of GSH ranges from 1 mM to 15 mM[38,

39], it was expected that MMCNP uptaken by the cancer cells should release its cargo within an hour. The observed spectral features of the "ON" state Qdots (i.e. after release from MMCNP) (Fig. 2) were in good agreement with those of Qdots in solution as shown in Fig. S3b. The STAT3 inhibitor is also a fluorescent molecule (λ_{ex}: 300 nm and λ_{em}: 396 nm) of which the fluorescence was quenched in MMCNPs (Fig. 3). These data of Fig. 3 show that full restoration of STAT3 fluorescence occurred within one hour, after which no further increase in STAT3 fluorescence intensity was observed. The inset of the Fig. 3 shows a plot of STAT3 fluorescence intensity measured at the peak emission wavelength (430 nm) as a function of time. This plot illustrated that the fluorescence intensity plateaus at 60 minutes. Both IONP and Qdots can quench the fluorescence of STAT3 drug via electron and/or energy transfer processes. Restoration of STAT3 drug emission was observed once MMCNPs were treated with GSH in solution (Fig. 3) was thus confirming disintegration of MMCNPs and release of STAT3 inhibitors.

To validate the proof-of-concept, we challenged the MMCNP against the intracellular GSH environment where the reported GSH concentration was in the millimolar (mM) range, typically between 2 mM and 15 mM[38, 39]. The human breast cancer (MDA-MB-231) cell line, known to over-express folate receptors[41], and the mouse thymus stromal epithelial cell line (TE-71) were incubated for up to 24 hrs with MMCNP at a concentration of 50 μg/mL. As expected, a significant uptake of folate conjugated MMCNP by the cancer cells was observed compared to normal cells as shown in Fig. 4. These results also showed that complete restoration of fluorescence occurred within 3 hr incubation (Fig. 4a). This confirmed extensive folate receptor mediated uptake of the MMCNPs. MDA-MB-231 cells incubated with MMCNPs for 24 hours, again was showing significant Qdot fluorescence that was similar to the 3 hour incubation experiment (Fig. 4b). These data show that uptake of MMCNPs and subsequent restoration of Qdot fluorescence (indicative of STAT3 release) occurred in less than 3 hours. The control experiment performed with MDA-MB-231 cells to which no MMCNPs were added (Fig. 4c). As expected only a minor cellular autofluorescence was observed. We performed another control experiment with mouse thymus stromal epithelial cells, TE-71 incubated with MMCNPs for 24 hours (Fig. 4d). Similar to the control experiment shown in Fig. 4c, only background autofluorescence was observed at locations that correspond to the locations of the cells, with no evidence of uptake of MMCNPs by the TE-71 normal cells. This control experiment validated that the delivery of MMCNPs was highly targeted to MDA-MB-231 cells, which over-expresses folate receptors. Restoration of fluorescence in cancer cells was a direct confirmation of targeted cellular uptake of MMCNPs and subsequent disintegration of MMCNP into the separate components i.e. IONP, Qdots, and release of ligands including drug molecules.

Systematic optical studies were performed to investigate intracellular drug release at the single cell level (Fig. 5). Confocal microscopy images of the MDA-MB-231 cells incubated with MMCNPs for 5 hrs (Fig. 5a and Fig. 5b) clearly show that MMCNP were uptaken by the cells. In addition, strong fluorescence signal from only a few locations in the cell can be observed. These data show that Qdots were released from the MMCNP through the cleavage of disulfide bonds by GSH (see Scheme 1). Besides the images of single cells incubated with MMCNP, emission spectra of different regions in single cells were also collected (Fig. 5c, red and cyan lines). The Qdots in the intracellular environment show emission spectra were red-shifted and broadened with respect to uncoated free Qdots in solution (Fig. S3b). These spectral differences were attributed to aggregation of the Qdots after release from MMCNP in the cytosol. This observation was confirmed with solution experiments on bare Qdots by observing emission spectra before and after aggregation, as well as addition of GSH to each of these samples (data not shown). We found from control experiments that addition of GSH to a suspension of bare Qdots leads to a stable Qdot suspension and has no noticeable effect on the Qdot emission properties (data not shown). These observations may

provide preliminary indication that in the intracellular environment GSH does not necessarily exchange with the NAC/cargo-ligand that is initially present on the Qdot surface due to the fact that intracellular Qdot aggregation is observed after cargo release, although it could be argued that binding constants of both molecules could be comparable given that GSH and NAC both contain a single thiol group in their structure (monodentate ligand). However, to conclusively determine the mechanism of removal of the NAC-ligands from the Qdot surface by GSH further investigations need to be performed, which are planned for the near future. The observation of only a few very bright spots in a single cell in the fluorescence images indicates aggregation of multiple Qdots in a single or a few clusters. The Qdot aggregation is reasonable given that while in the MMCNP Qdots are stabilized by PEG coating, after exposure to GSH this coating is removed by cleavage of disulfide bonds, resulting in hydrophobic Qdots that self-aggregate. In addition, the data show that these Qdot aggregates preferentially localize near the cell membrane, again due to their hydrophobic nature. Other locations where Qdot aggregates are not present only show autofluorescence. It should be noted that while the STAT3 drug itself is also fluorescent (Fig. 2b), the experiments on intracellular delivery cannot be reliably performed by measuring the STAT3 drug fluorescence due to weak fluorescence and the presence of cellular auto-fluorescence, hence the need for the optical signal of the Qdots. We performed the normalized ensemble fluorescence emission spectra acquired by sample scanning laser confocal microscopy under 375 nm laser excitation (Fig. 5c). The ensembles were constructed by averaging fluorescence emission spectra obtained at different locations inside individual cells under illumination with a diffraction limited laser spots (~ 300 nm). Spectra were acquired at the location of the Qdot aggregates (red line) and the cellular regions without Qdots (autofluorescence, dark cyan line). As a control, the same experiment was completed for Qdots in the “OFF state” (black line) and “ON state” (blue line) on glass substrates. Both the intracellular and extra-cellular “ON state” Qdots appear slightly red shifted with respect to the “OFF state” Qdots. In addition, the “ON state” Qdots were significantly broadened at the blue edge as well as the red edge of the spectra, possibly due to the presence of GSH on the Qdot surface. The difference in the appearance of the red shoulders in the intracellular and extra-cellular “ON state” Qdots is most likely due to difference in the environment. The spectral feature around 500 nm in the intracellular “ON state” Qdot fluorescence emission ensemble spectrum is due the contribution of cellular autofluorescence.

To demonstrate the concept of multimodality of the MMCNPs, an agar phantom was prepared using a 10 mm NMR tube (Fig. 6) for MRI and optical imaging studies. Fig. 6a shows the schematic of agar phantom design. The bottom part of the tube contains only MDA-MB-231 cells (as a control), middle part contains only MMCNPs (as a control) and the top part of the tube contains the same cells loaded with MMCNPs. All of these were dispersed in 3% agarose gel under same condition. A digital image of the tube was recorded under room light (Fig. 6b) as well as under illumination by a hand-held 366 nm multiband UV lamp (Fig. 6c). The unfiltered images clearly show a light brown color where cells are located in room light conditions whereas an intense red color appears due to Qdot fluorescence under UV illumination. The MDA-MB-231 cells loaded with the MMCNPs emit red fluorescence that is clearly visible to the naked eye. Control cells do not show any detectable fluorescence emission. An MRI image of the phantom (Fig. 6d) clearly shows cell clusters that correlate well with the fluorescence image. A 3D reconstruction of the MR images is provided in the supplementary section (Fig. S5). This demonstrated the appearance of strong MRI signal from the MDA-MB-231 cells loaded with the MMCNPs (indicated with false red color) in contrast with the control cells.

The CyQUANT™ cell proliferation assay was used in a comparative cell viability study to determine cytotoxicity of MMCNPs without STAT3 drug (control particle), STAT3 drug

itself, and MMCNPs with STAT3 conjugation. Two cancer cell lines, MDA-MB-231 and pancreatic (Panc-1) cancer cells were used along with mouse thymus stromal epithelial TE-71 cells (control). Results (Fig. 7) suggest that MMCNPs (with STAT3) treated cancer cells have lower viability than cells treated with free STAT 3 drug when MMCNP and STAT3 were administered to the cell medium at identical concentrations. Compared to untreated (control), the viability of cells treated with MMCNPs to which no STAT3 is attached (RII 61) was attached is not significantly different, indicating that the MMCNP itself do not compromise cell viability. By contrast, the cells treated with 50 μM STAT3 inhibitor only (drug) showed a 15–20% decrease in cell viability, while cells treated with fully functional MMCNPs to which STAT3 inhibitor was attached showed nearly 30% decrease in cell viability, even though the amount of STAT3 inhibitor contained in the 5 μg of MMCNP administered in 100 μL of cell media was expected to release a far less amount of the STAT3 inhibitor than the 50 μM that was directly added to the cells in the other study. This key observation demonstrates the effectiveness of the reported nanoparticle design in highly targeted drug delivery to the cancer cells, while maximizing cancer cell death with reduced amounts of drugs used compared to conventional approaches. Even though the MMCNPs consume much less STAT3 drug, the delivery efficiency is dramatically increased, thus resulting in increased therapeutic efficiency while minimizing the potential for medical side effects due to presence of excess free drug.

4. Conclusion

Quantum dot (Qdot)-iron oxide (IO) based multimodal/multifunctional nanocomposite probe that is optically and magnetically imageable, targetable and capable of reporting on intracellular drug release events has been reported herein. By design, the present nanoparticle system has multimodalities (optically and magnetically active) and multifunctionalities (i.e. imaging, targeting, drug delivery) that are current state-of-the-art in nanomedicine research[1, 8, 14, 19–21, 23, 28–31]. In addition, the MMCNP discussed here integrate sensing modalities that report on the event as well as the location of intracellular release of cargo. The impact and implications of this new development along with the traditional multimodalities and multifunctionalities are immediate for drug discovery and cancer biology.

Supplementary Material

Refer to Web version on PubMed Central for supplementary material.

Acknowledgments

S.S. and G.A.W. acknowledge the National Science Foundation (NSF-NIRT Grant EEC-0506560) and National Institutes of Health (grant # 2P01HL059412-11A1). JT and P.T.G. acknowledges the National Institutes of Health grants CA106439 and CA128865. M.D. and A.G. gratefully acknowledge the National Science Foundation (NSF) for financial support of this work through CAREER award CBET-0746210.

References

[1]. Ferrari M. Cancer nanotechnology: Opportunities and challenges. Nat Rev Cancer. 2005; 5:161–71. [PubMed: 15738981]

[2]. Peer D, Karp JM, Hong S, FaroKhzad OC, Margalit R, Langer R. Nanocarriers as an emerging platform for cancer therapy. Nat Nanotechnol. 2007; 2:751–60. [PubMed: 18654426]

[3]. Foy SP, Manthe RL, Foy ST, Dimitrijevic S, Krishnamurthy N, Labhasetwar V. Optical Imaging and Magnetic Field Targeting of Magnetic Nanoparticles in Tumors. ACS Nano. 2010; 4:5217–24. [PubMed: 20731413]

[4]. John R, Rezaeipoor R, Adie SG, Chaney EJ, Oldenburg AL, Marjanovic M, et al. In vivo magnetomotive optical molecular imaging using targeted magnetic nanoprobes. Proc Natl Acad Sci U S A. 2010; 107:8085–90. [PubMed: 20404194]

[5]. Lee JH, Lee K, Moon SH, Lee Y, Park TG, Cheon J. All-in-One Target-Cell-Specific Magnetic Nanoparticles for Simultaneous Molecular Imaging and siRNA Delivery. Angew Chem Int Ed Engl. 2009; 48:4174–9. [PubMed: 19408274]

[6]. Mulder WJM, Strijkers GJ, Van Tilborg GAF, Cormode DP, Fayad ZA, Nicolay K. Nanoparticulate Assemblies of Amphiphiles and Diagnostically Active Materials for Multimodality Imaging. Acc Chem Res. 2009; 42:904–14. [PubMed: 19435319]

[7]. Park K, Lee S, Kang E, Kim K, Choi K, Kwon IC. New Generation of Multifunctional Nanoparticles for Cancer Imaging and Therapy. Adv Funct Mater. 2009; 19:1553–66.

[8]. Kircher MF, Mahmood U, King RS, Weissleder R, Josephson L. A multimodal nanoparticle for preoperative magnetic resonance imaging and intraoperative optical brain tumor delineation. Cancer Res. 2003; 63:8122–5. [PubMed: 14678964]

[9]. McCann CM, Waterman P, Figueiredo JL, Aikawa E, Weissleder R, Chen JW. Combined magnetic resonance and fluorescence imaging of the living mouse brain reveals glioma response to chemotherapy. Neuroimage. 2009; 45:360–9. [PubMed: 19154791]

[10]. Shi D, Cho HS, Chen Y, Xu H, Gu H, Lian J, et al. Fluorescent Polystyrene–Fe_3O_4 Composite Nanospheres for In Vivo Imaging and Hyperthermia. Adv Mater. 2009; 21:2170–3.

[11]. Lee J-H, Schneider B, Jordan EK, Liu W, Frank JA. Synthesis of Complexable Fluorescent Superparamagnetic Iron Oxide Nanoparticles (FL SPIONs) and Cell Labeling for Clinical Application. Adv Mater. 2008; 20:2512–6. [PubMed: 19578472]

[12]. Liu Z, Lammers T, Ehling J, Fokong S, Bornemann J, Kiessling F, et al. Iron oxide nanoparticle-containing microbubble composites as contrast agents for MR and ultrasound dual-modality imaging. Biomaterials. 2011; 32:6155–63. [PubMed: 21632103]

[13]. Tan YF, Chandrasekharan P, Maity D, Yong CX, Chuang K-H, Zhao Y, et al. Multimodal tumor imaging by iron oxides and quantum dots formulated in poly (lactic acid)-d-alpha-tocopheryl polyethylene glycol 1000 succinate nanoparticles. Biomaterials. 2011; 32:2969–78. [PubMed: 21257200]

[14]. Erogbogbo F, Yong KT, Hu R, Law WC, Ding H, Chang CW, et al. Biocompatible Magnetofluorescent Probes: Luminescent Silicon Quantum Dots Coupled with Superparamagnetic Iron(III) Oxide. ACS Nano. 2010; 4:5131–8. [PubMed: 20738120]

[15]. Mulder WJM, Castermans K, van Beijnum JR, Egbrink M, Chin PTK, Fayad ZA, et al. Molecular imaging of tumor angiogenesis using alpha v beta 3-integrin targeted multimodal quantum dots. Angiogenesis. 2009; 12:17–24. [PubMed: 19067197]

[16]. Mulder WJM, Strijkers GJ, Nicolay K, Griffioen AW. Quantum dots for multimodal molecular imaging of angiogenesis. Angiogenesis. 2010; 13:131–4. [PubMed: 20552267]

[17]. Trehin R, Figueiredo JL, Pittet MJ, Weissleder R, Josephson L, Mahmood U. Fluorescent nanoparticle uptake for brain tumor visualization. Neoplasia. 2006; 8:302–11. [PubMed: 16756722]

[18]. Das M, Mishra D, Dhak P, Gupta S, Maiti TK, Basak A, et al. Biofunctionalized, Phosphonate-Grafted, Ultrasmall Iron Oxide Nanoparticles for Combined Targeted Cancer Therapy and Multimodal Imaging. Small. 2009; 5:2883–93. [PubMed: 19856326]

[19]. Zrazhevskiy P, Sena M, Gao XH. Designing multifunctional quantum dots for bioimaging, detection, and drug delivery. Chem Soc Rev. 2010; 39:4326–54. [PubMed: 20697629]

[20]. Cheng SH, Lee CH, Chen MC, Souris JS, Tseng FG, Yang CS, et al. Tri-functionalization of mesoporous silica nanoparticles for comprehensive cancer theranostics-the trio of imaging, targeting and therapy. J Mater Chem. 2010; 20:6149–57.

[21]. Medintz IL, Stewart MH, Trammell SA, Susumu K, Delehanty JB, Mei BC, et al. Quantum-dot/dopamine bioconjugates function as redox coupled assemblies for in vitro and intracellular pH sensing. Nat Mater. 2010; 9:676–84. [PubMed: 20651808]

[22]. Medintz IL, Clapp AR, Brunel FM, Tiefenbrunn T, Uyeda HT, Chang EL, et al. Proteolytic activity monitored by fluorescence resonance energy transfer through quantum-dot-peptide conjugates. Nat Mater. 2006; 5:581–9. [PubMed: 16799548]

[23]. Medintz IL, Uyeda HT, Goldman ER, Mattoussi H. Quantum dot bioconjugates for imaging, labelling and sensing. Nat Mater. 2005; 4:435–46. [PubMed: 15928695]

[24]. Medintz IL, Clapp AR, Mattoussi H, Goldman ER, Fisher B, Mauro JM. Self-assembled nanoscale biosensors based on quantum dot FRET donors. Nat Mater. 2003; 2:630–8. [PubMed: 12942071]

[25]. Banerjee S, Kar S, Perez JM, Santra S. Quantum Dot-Based OFF/ON Probe for Detection of Glutathione. J Phys Chem C. 2009; 113:9659–63.

[26]. Banerjee S, Kar S, Santra S. A simple strategy for quantum dot assisted selective detection of cadmium ions. Chem Commun (Camb). 2008:3037–9. [PubMed: 18688340]

[27]. Bagalkot V, Zhang L, Levy-Nissenbaum E, Jon S, Kantoff PW, Langer R, et al. Quantum dot - Aptamer conjugates for synchronous cancer imaging, therapy, and sensing of drug delivery based on Bifluorescence resonance energy transfer. Nano Lett. 2007; 7:3065–70. [PubMed: 17854227]

[28]. Bagalkot V, Zhang L, Levy-Nissenbaum E, Jon S, Kantoff PW, Langer R, et al. Quantum dot - Aptamer conjugates for synchronous cancer imaging, therapy, and sensing of drug delivery based on Bifluorescence resonance energy transfer. Nano Lett. 2007; 7:3065–70. [PubMed: 17854227]

[29]. Gao JH, Gu HW, Xu B. Multifunctional Magnetic Nanoparticles: Design, Synthesis, and Biomedical Applications. Acc Chem Res. 2009; 42:1097–107. [PubMed: 19476332]

[30]. Liong M, Lu J, Kovochich M, Xia T, Ruehm SG, Nel AE, et al. Multifunctional inorganic nanoparticles for imaging, targeting, and drug delivery. Acs Nano. 2008; 2:889–96. [PubMed: 19206485]

[31]. Mulder WJM, Griffioen AW, Strijkers GJ, Cormode DP, Nicolay K, Fayad ZA. Magnetic and fluorescent nanoparticles for multimodality imaging. Nanomedicine. 2007; 2:307–24. [PubMed: 17716176]

[32]. Zhang XL, Yue PB, Fletcher S, Zhao W, Gunning PT, Turkson J. A novel small-molecule disrupts Stat3 SH2 domain-phosphotyrosine interactions and Stat3-dependent tumor processes. Biochem Pharmacol. 2010; 79:1398–409. [PubMed: 20067773]

[33]. Fletcher S, Singh J, Zhang X, Yue PB, Page BDG, Sharmeen S, et al. Disruption of Transcriptionally Active Stat3 Dimers with Non-phosphorylated, Salicylic Acid-Based Small Molecules: Potent in vitro and Tumor Cell Activities. Chembiochem. 2009; 10:1959–64. [PubMed: 19644994]

[34]. Siddiquee K, Zhang S, Guida WC, Blaskovich MA, Greedy B, Lawrence HR, et al. Selective chemical probe inhibitor of Stat3, identified through structure-based virtual screening, induces antitumor activity. Proc Natl Acad Sci U S A. 2007; 104:7391–6. [PubMed: 17463090]

[35]. Jones G, Willett P, Glen RC, Leach AR, Taylor R. Development and validation of a genetic algorithm for flexible docking. J Mol Biol. 1997; 267:727–48. [PubMed: 9126849]

[36]. Robineau M, Zins D. Surfactant-coated particles in magnetic fluids. Characterization and study of thermal stability under inert atmosphere. Ann Chimie Sci Materiaux. 1995; 20:327–33.

[37]. Santra S, Yang HS, Holloway PH, Stanley JT, Mericle RA. Synthesis of water-dispersible fluorescent, radio-opaque, and paramagnetic CdS : Mn/ZnS quantum dots: A multifunctional probe for bioimaging. J Am Chem Soc. 2005; 127:1656–7. [PubMed: 15700997]

[38]. Tietze F. Enzymic method for quantitative determination of nanogram amounts of total and oxidized glutathione - applications to mammalian blood and other tissues. Anal Biochem. 1969; 27:502–&. [PubMed: 4388022]

[39]. Coles B, Ketterer B. The role of glutathione and glutathione transferases in chemical carcinogenesis. Crit Rev Biochem Mol Biol. 1990; 25:47–70. [PubMed: 2182291]

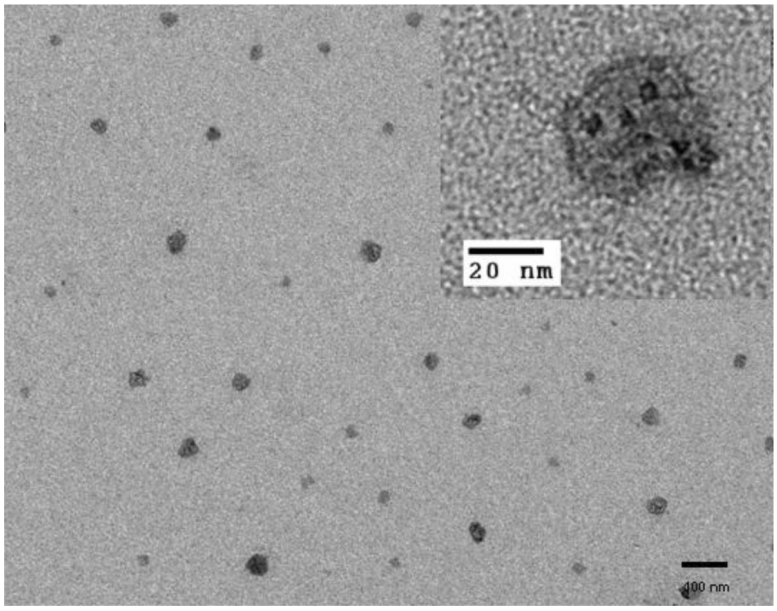

Fig.1.
TEM image of MMCNPs are showing nearly spherical particles with irregular surface morphology indicative of the presence of satellite Qdots on the IONPs.

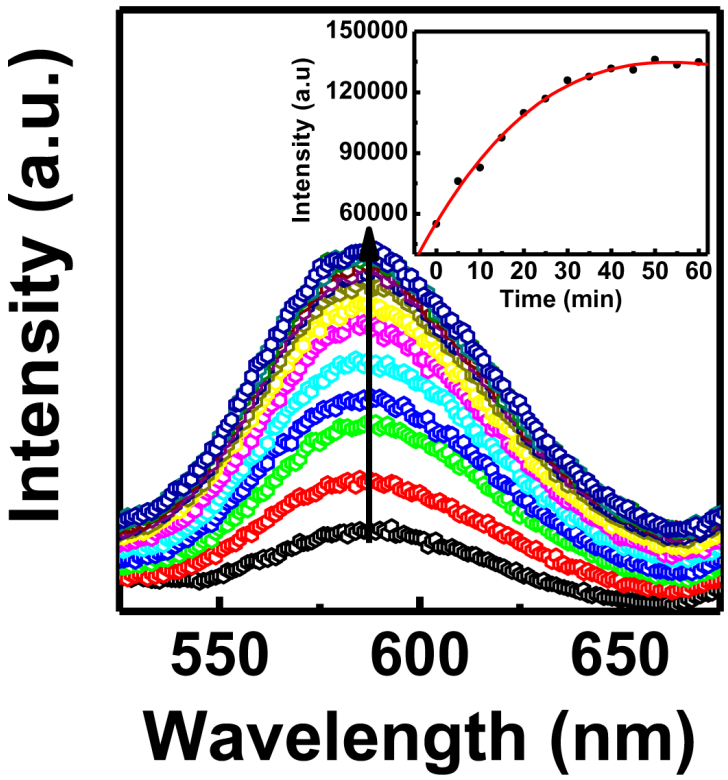

Fig. 2.
Qdot fluorescence emission spectra (excitation wavelength = 375 nm) measured as a function of time at 7.0 mM GSH concentration. The red line is a non-linear fit to the data.

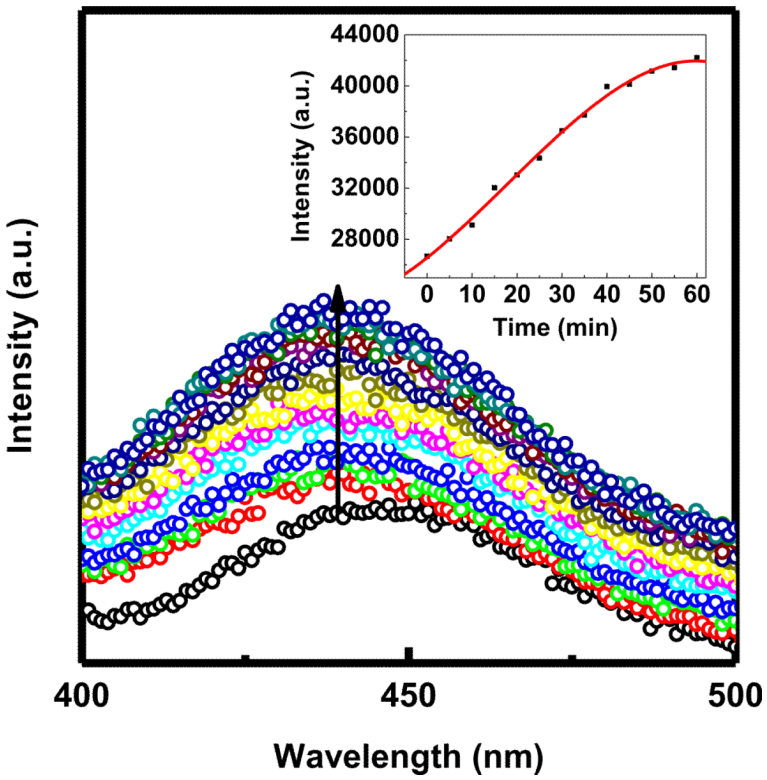

Fig. 3.
STAT3 fluorescence emission spectra (excitation wavelength = 300 nm) measured as a function of time at 7.0 mM GSH concentration. The red line is a non-linear fit to the data.

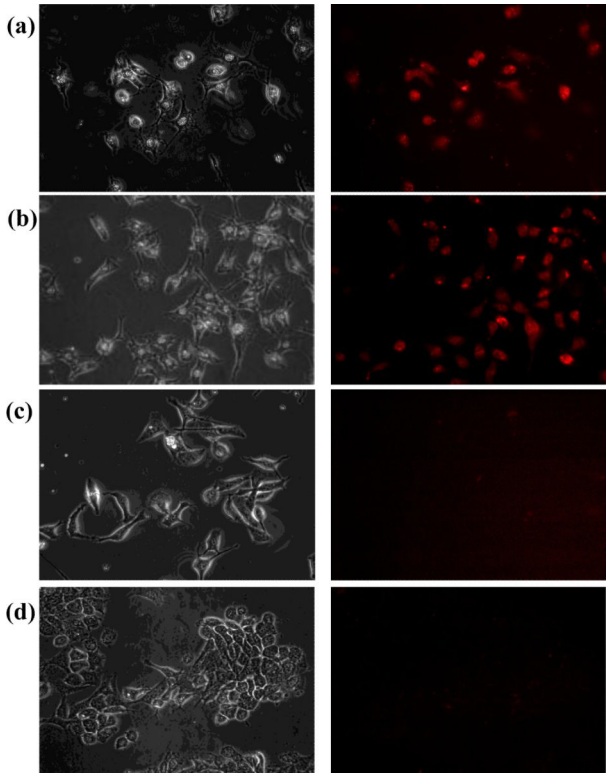

Fig. 4.

Phase-contrast (left panel) and corresponding epi-fluorescence (right panel) microscopy images: (a) MDA-MB-231 cells incubated with MMCNPs for 3 hours, showing significant Qdot fluorescence; (b) MDA-MB-231 cells incubated with MMCNPs for 24 hours, again showing significant Qdot fluorescence that is similar to the 3 hour incubation experiment; (c) control experiment performed with MDA-MB-231 cells to which no MMCNP were added; (d) control experiment performed with mouse thymus stromal epithelial cells, TE-71 incubated with MMCNPs for 24 hours.

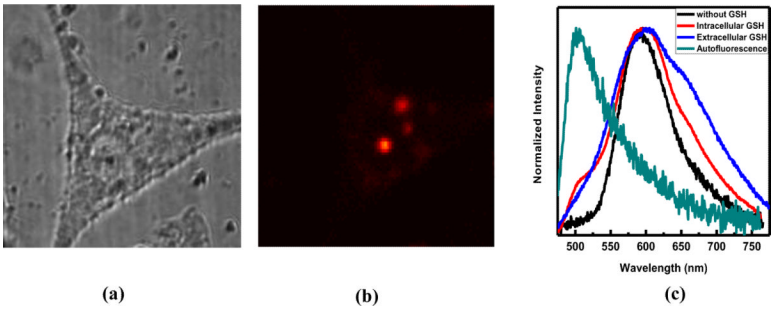

Fig. 5.

(a) Bright field; (b) corresponding epi-luminescence laser microscopy images of MDA-MB-231 cells incubated with MMCNPs for 5 hours; (c) Normalized ensemble fluorescence emission spectra acquired by sample scanning laser confocal microscopy under 375 nm laser excitation.

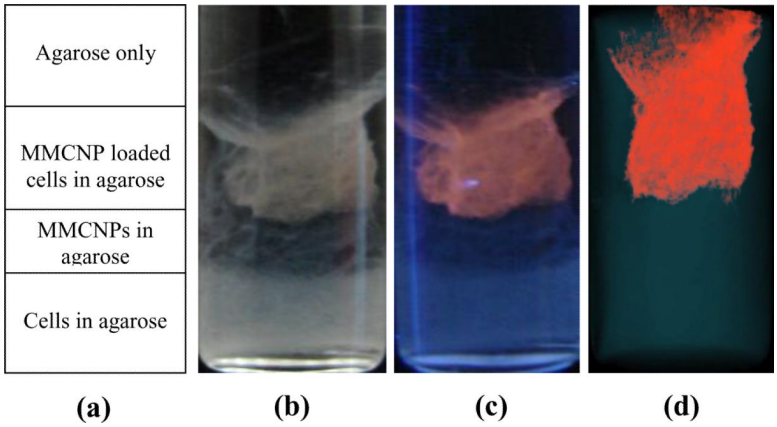

Fig. 6.

(a) Schematic of agar phantom design. The agar phantom consists of four layers. From bottom to top these layers are: MDA-MB-231 cells embedded in agar (control), MMCNPs embedded in agar (control); MDA-MB-231 cells loaded with the MMCNPs embedded in agar (sample) and agar layer, respectively; (b) digital photograph of agar phantom; (c) Corresponding digital photograph of agar phantom under 366 nm multiband UV irradiation; (d) MRI image of agar phantom.

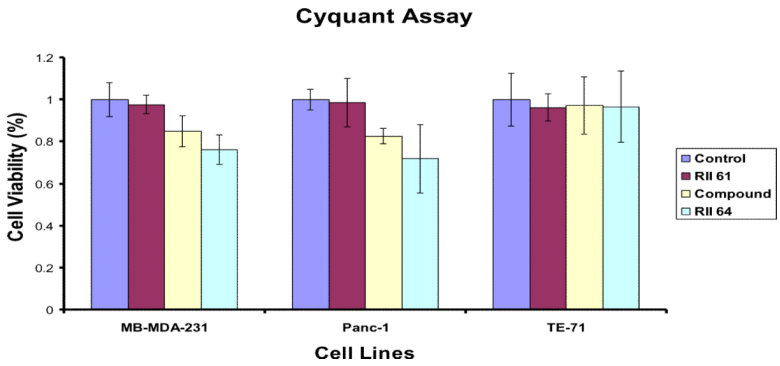

Fig. 7.

CyQuant® cell viability assay performed on the human breast (MB-MDA-231) and pancreatic (Panc-1) cancer lines, or the mouse thymus stromal epithelial line, TE-71. Cells were untreated (control) or treated for 24 hours with MMCNPs to which no STAT3 inhibitor was attached (RII 61), STAT3 inhibitor only (compound), and MMCNPs (RII 64).

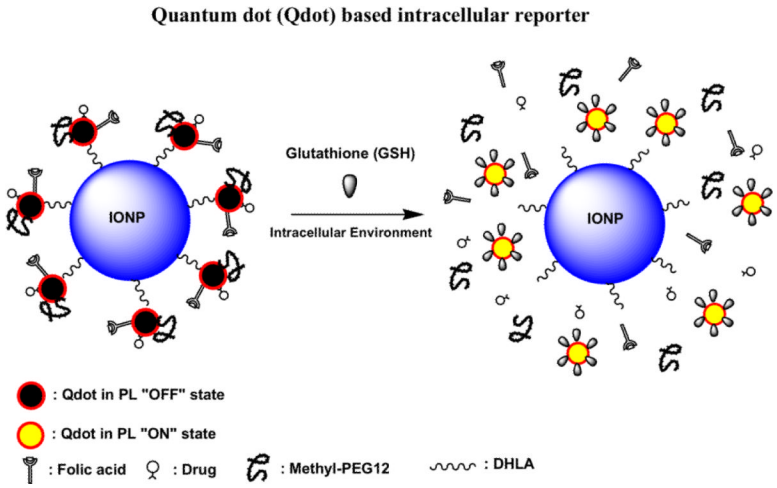

Scheme 1.
Schematic representation of MMCNP in “OFF state” and “ON state”.